Far-infrared perfect optical absorption in film supporting metallic grating structures

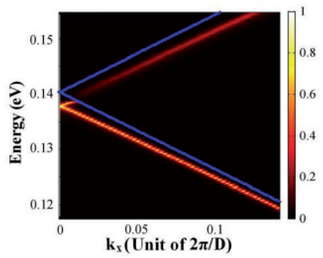

Absorción óptica perfecta de la radiación infrarroja lejana en estructuras de parrilla metálica soportadas por una película

Xiumei Chen[1], Xiaopeng Yan[1,*], Ping Li[1], and Wenqiang Wang[2]

[1] Science and Technology on Electromechanical Dynamic Control Laboratory, Beijing Institute of Technology, Zhongguancun South Street 5#, Beijing, 100081, China. * Corresponding author, email: yanxiaopeng@bit.edu.cn

[2] Center for Nanoscience and Nanotechnology and School of Physics and Technology, Wuhan University, Luojiashan, Wuhan, 430072, Hubei, China

DOI: http://dx.doi.org/10.6036/8176 | Recibido: 10/10/2016 • Evaluado: 11/10/2016 • Aceptado: 30/12/2016

RESUMEN

- Se demuestra la absorción óptica perfecta (POA) de la región infrarroja lejana en una estructura de rejilla metálica para baja longitud de onda sobre una película dieléctrica de apoyo y se investigan las características de la POA por cálculo teórico y por análisis bajo luz incidente transversal polarizada magnéticamente. En este estudio, se propuso por primera vez un diseño estructural sencillo para lograr la casi perfecta absorción en la región del infrarrojo lejano. La dependencia de la POA en la geometría se calculó mediante un riguroso análisis de ondas acopladas. Además, se investigaron el campo electromagnético, las distribuciones de densidad de flujo de energía y la dispersión de la absorción para la POA por simulaciones numéricas. Los resultados muestran que la POA en la región del infrarrojo lejano se obtiene utilizando una estructura de rejilla metálica soportada por película con las ventajas de una sintonización lineal de la longitud de onda del POA y un diseño estructural sencillo con una gran tolerancia geométrica. Además de los modos de resonancia de Fabry-Perot en las rendijas de la rejilla y de los plasmones polaritones de superficie excitados sobre las superficies, se demostraron también los modos de guía de ondas en la película en el caso de película gruesa, lo que cambia significativamente la región de pérdida de energía, pero con un efecto insignificante en el ancho del pico resonante de la POA. Las ventajas de la sintonización lineal de la longitud de onda, el diseño estructural sencillo y la gran tolerancia geométrica de la POA en la región del infrarroja lejano demuestran su aplicación prometedora en la detección, detección y modulación de la radiación infrarroja .
- **Palabras clave:** Absorción, Plasmón Polaritones de Superficie, Estructura de Rejilla para Baja Longitud de Onda, Modos de Guía de Ondas.

ABSTRACT

Perfect optical absorption (POA) in the far-infrared region is demonstrated in the subwavelength metallic grating structure with a supporting dielectric film, and the features of the POA are investigated by theoretical calculation and analysis under normal transverse magnetic polarized incident light. In this study, a simple structure design was first proposed to achieve nearly perfect absorption in the far-infrared region. The dependence of the POA on the geometry was calculated by rigorous coupled wave analysis. Furthermore, the electric field and energy flow density distributions and absorption dispersion for the POA were investigated by numerical simulations. Results show that the POA in the far-infrared region is obtained using the film supporting metallic grating structure with the advantages of linear tunability on the POA wavelength and simple structure design with a large geometric tolerance. The waveguide modes in the film is demonstrated to play an important role for the perfect absorption, which significantly change the energy loss region, but with negligible effect on the POA resonant peak width, besides the Fabry-Perot resonant modes in the grating slits and the surface plasmon polaritons excited on the surfaces. The advantages of wavelength linear tunability, simple structure design, and large geometric tolerance of the POA in the far-infrared region demonstrate its promising application in infrared sensing, detection, and modulation.

Keywords: Absorption, Surface plasmon polaritons, Subwavelength grating structure, Waveguide modes.

1. INTRODUCTION

Perfect optical absorption (POA) in microstructures/nanostructures has attracted considerable attention because of its potential applications in sensing, detection, photovoltaics and modulation. The phenomenon has been investigated for several decades since enhanced absorption was first demonstrated by metallic gratings in 1976 [1]. Many grating structures have been designed to obtain the perfect absorption, and several mechanisms have been presented to explain the phenomenon in recent years. Thus far, most of POA designs and features are studied in the visible region. Only a few designs for the POA have been reported in the infrared region; even less in the far-infrared region. Considering the important role of the absorption efficiency on the detection sensitivity, and far-infrared is an important band for the infrared sensor and detector, it is significant to realize the POA in the far-infrared region for the applications of infrared sensing and detection. Furthermore, it is also valuable to investigate the features of the POA in the far-infrared region because of the big difference in the metallic behaviors in the visible and far-infrared regions.

2. STATE OF THE ART

POA is near total absorption of the incident energy by modeling structures to suppress both transmission and reflection to approach zero. Since the enhanced absorption by grating structures was observed, various designs were proposed to achieve the perfect absorption, such as lamellar gratings [2], crossed gratings [3], and metallic gratings [4-6]. And many POA designs have been

used in the applications of solar cells [7, 8], resonance sensing [9], photodetectors [10], and thermal emitters [11]. Recently, the utilizations of hot electrons generated by surface plasmon decay further boost the interesting in catalysis, therapy, detection, and photovoltaics [12]. On the other hand, the phenomenon of the enhance absorption were also studied based on different designs, which were explained as the excitation of surface plasmon polaritons (SPPs) on corrugated metallic-dielectric surfaces [13, 14, 15], the Fabry-Perot (FP) resonant modes [16, 22], and the coupling of electric and magnetic responses in metamaterials [17, 18].

The infrared absorbing component is an important part of infrared sensor and detector and the maximum infrared absorption efficiency of the traditional infrared absorbing material such as gold film is only approximately 50% [19]. To improve the absorption efficiency of the absorbing component is one of the effective methods to improve the detection efficiency [19]. Hence, the investigation of the enhanced absorption for the infrared materials was also considered in recent years. So far, several compound multilayer structures were designed for the infrared perfect absorption, such as two-dimensional structures for near-infrared [20, 21] and mid-infrared [10] and seven-layer one-dimensional structure for far-infrared [22]. The metamaterial was also considered for the perfect absorption in the mid-infrared region [17]. Furthermore, a single-layer structure with rectangular grooves [23] was designed for near-infrared. In view of the microfabrication process, the multilayer design makes the structure difficult to integrate the layers together, and the metamaterial is more complicated than metallic gratings. Although, the single-layer is really simpler on the structure form than aforementioned multilayer structures, it is also difficult in practical fabrication because of the freestanding design and embedded rectangular grooves. The features of the POA in infrared region were also investigated with different designs, which were explained as SPPs [20, 21], FP modes [22], and horizontal surface plasmons at the horizontal metallic boundaries and vertical cavity modes inside the slits [23]. Overall, only a seven-layer structure was designed for far-infrared perfect absorption which is difficult to fabricate, and the mechanism of the POA in different structure designs are not totally in agreement. Therefore, it is important to design a real simple structure for the POA in the far-infrared region considering both structure form and microfabrication process. And it is also valuable to study the features of the POA in the new structure design.

The remainder of this paper is organized as follows. Section 3 introduces the grating structure model and the theoretical calculation and analysis method. Section 4 describes and analyzes the results of POA dependence on the geometry, electric field and energy flow density distributions, and absorption dispersion. Section 5 summarizes the conclusions.

3. METHODOLOGY

3.1. GRATING STRUCTURE MODEL

The subwavelength structure model is selected as the two-layer metallic grating structure with a supporting dielectric film because it is simple on both structure form and microfabrication process which can be considered as one advantage of the structure design. This structure is regarded as air/grating/film/air with air as the filling material in the grating slits. The dielectric film is attached to the bottom of the grating as a supporting film. The schematic of the film supporting grating structure is shown as in Fig. 1, together with the coordinate system and the geometry notations. The incident vector lies in the xOy plane from above with the magnetic field oriented perpendicular to the propagation direction, i.e., transverse magnetic (TM) polarization. The normal incident light is considered, with the angle of incidence measured from the surface normal as θ = 0, i.e., the magnetic field vector is parallel to the grating line direction. The grating period (*D*), grating thickness (*T*), grating width (*w*), slit width (*s*) (slit ratio *k=s/D*), and supporting dielectric film thickness (T_d) are the important grating structure geometric parameters.

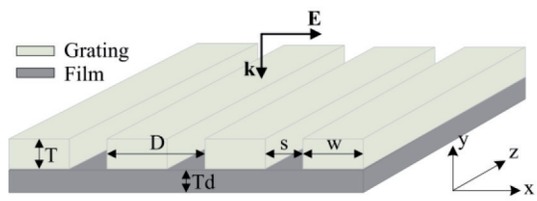

Fig. 1: Schematic of the film supporting grating structure

Given that the metal permittivity changes with the incident light wavelength, the permittivity of the metallic grating is calculated using the Drude model expressed in Eq. (1):

$$\varepsilon = \varepsilon_\infty - \frac{\omega_p^2}{\omega^2 + i\omega\gamma} = \varepsilon_\infty - \frac{\omega_p^2}{\omega^2 + \gamma^2} + i\frac{\omega_p^2\gamma}{\omega(\omega^2 + \gamma^2)} \tag{1}$$

where ω is the frequency of the incident light. Gold is selected as the metallic material of the grating, which is often used as the metal for surface plasmon excitation because of its low loss and stability. The permittivity of gold is calculated using the Drude model [24], with the following relevant coefficients in Eq. (1) as $\varepsilon_\infty = 1$, $\omega_p = 1.15 \times 10^{16}\ s^{-1}$, and $\gamma = 0.9 \times 10^{14}\ s^{-1}$. The refractive index of the supporting dielectric film is taken 1.4 for example, which approximately represents silica in the infrared wavelength.

3.2. THEORETICAL CALCULATION AND ANALYSIS METHOD

The ratios of reflection, transmission, and absorption are related to the incident light wavelength, incident angle, grating structure geometric parameters, and material permittivity. The transmittance and reflectance of p-order diffraction under the TM-polarized incident light are calculated as follows:

$$R_p = \delta_{0,p} - \frac{\omega/c}{\alpha_p} g_p (A - B_u) \tag{2}$$

$$T_p = \frac{\omega/c}{\alpha_p} g_p (A_u - B) \tag{3}$$

where $\delta_{o,p}$ is the Kronecker function with $\delta_{o,p} = 1$ when $p = 0$ and $\delta_{o,p} = 0$ when $p \neq 0$. When the incident wavelength is more than the grating period with $g_o = 0$ and $\alpha_o = \omega/c$ in the case of normal incident light, the transmittance and reflectance of zero-order diffraction are $r_0 = 1-(A-B_u)$ and $t_0 = A-B_u$. The total absorption of the metallic grating structures is derived as follows:

$$A = 1 - \sum_{p=-\infty}^{\infty} R_p - \sum_{p=-\infty}^{\infty} T_p \tag{4}$$

So the absorption is defined as $A = 1-T-R$, where T is the transmittance and R is the reflectance, with T/R as the sum of T_p/R_p for all propagation orders. The reflection and transmission are cal-

culated using the rigorous coupled wave analysis (GD-Calc [25]). The diffraction orders up to 100 are considered to achieve good convergence.

According to the principle of energy conservation, the absorption is the result from the energy loss in the grating structure. From the Poynting theorem [26]:

$$\frac{\partial u}{\partial t}+\nabla\cdot\mathrm{S}=-\mathrm{J}\cdot\mathrm{E} \tag{5}$$

The energy loss in the grating structure is caused by the work down of the electromagnetic forces on the electric charges, where **S** is the Poynting vector, u is the electromagnetic energy density, and J is the total current density. To calculate and visualize the electric field and energy flow density distributions are the effective ways to explain the physical mechanism of the perfect absorption.

The maximum absorption efficiencies of several specific incident wavelengths in the far-infrared region were calculated with the optimized geometric parameters firstly in order to confirm the perfect absorption can be achieved in this two-layer grating structure for far-infrared. Secondly, the dependence of the perfect absorption on geometric parameters and the refractive index of the supporting film were investigated in the far-infrared region. Finally, the electric field distribution, energy flow density distribution, and absorption dispersion were calculated and analyzed to explain the physical mechanism of the POA phenomenon. For the electric field and energy flow density distributions, a commercial finite differential time domain software (FDTD Solutions, Lumerical Solutions Inc., Vancouver, Canada) with nonuniform grids was used to calculate with the energy cutoff 10-5 for simulation convergence.

4. RESULT ANALYSIS AND DISCUSSION

4.1. ABSORPTION DEPENDENCE ON GEOMETRY

The maximum absorption efficiency of incident light in the metallic grating structure is obtained via suppressing the reflection and transmission by optimizing the structure parameters. Thus, the absorption dependence on the structure geometric parameter was investigated firstly. Fig. 2 shows the optical absorption spectrum curves with a single grating structure parameter changed as the grating slit width, grating thickness, film thickness, and grating period.

Firstly, the absorption efficiency was calculated with the varied slit ratio k from 0.04 to 0.6 by step size as 0.04, with other structure geometric parameters as the grating period D = 8.85 μm, grating thickness T = 1 μm, and film thickness Td = 0.5 μm. As shown in Fig. 2(a), the absorption peak redshifts when the absorption peak increased, then blueshifts when the absorption peak decreased. The maximum absorbance is 98.35% as nearly perfect absorption at wavelength 9.006 μm when k = 0.08. These phenomena can be explained by the behavior of FP resonant modes in the grating slits for the narrow and wide slits. When the slits are less than one third of the grating period, i.e., the narrow slit case, only a single fundamental transverse electromagnetic mode exists in the grating slits. Thus, the absorption peak redshifts with the slit increasing. When the scattering phase contributed by FP resonant modes achieves a certain value, the absorption efficiency approaches the maximum as the POA. By contrast, when the grating slits are larger than one third of the grating period, i.e., the wide slit case, more surface diffraction waves contribute to the surface plasmon modes and the absorption wavelength is near the grating period. More FP resonant modes exist in the grating slits in the wide slit case, which increase the radiation loss and reduce the absorption efficiency.

Next, the influence of the grating thickness on the absorption efficiency was studied as shown in Fig. 2(b). The grating thickness *T* is varied from 0.6 μm to 1.5 μm by step size as 0.1μm with other structure parameters as D = 8.85 μm, k = 0.086, and T_d = 0.5 μm. It can be observed that the absorption peak always redshifts when the grating thickness increased. This can be explained that the grating thickness affects the scattering phase contributed by the transverse electromagnetic mode in the grating slits, thus, the absorption peak redshifts with the increasing grating thickness.

In addition, the absorption dependence on the film thickness was also investigated as shown in Fig. 2(c). The film thickness T_d is varied from 0 μm to 3 μm by step size as 0.1 μm with other structure parameters as D = 8.85 μm, T = 1 μm *and* k = 0.086. It can be seen that the absorption peak also only redshifts when the film thickness increased. However, the absorption peak redshifts can't be explained by FP resonant mode in the slits as the grating thickness case. This phenomenon is due to the increasing phase contribution by multiple scattering waves inside the film and more electromagnetic mode contributions on the grating/film surface. Though it is not shown, we also calculated the absorption dependence on the refractive index of film, the changing trend of the absorption spectra is similar as it does with increasing film thickness. Thus, the refractive index of film material is not discussed

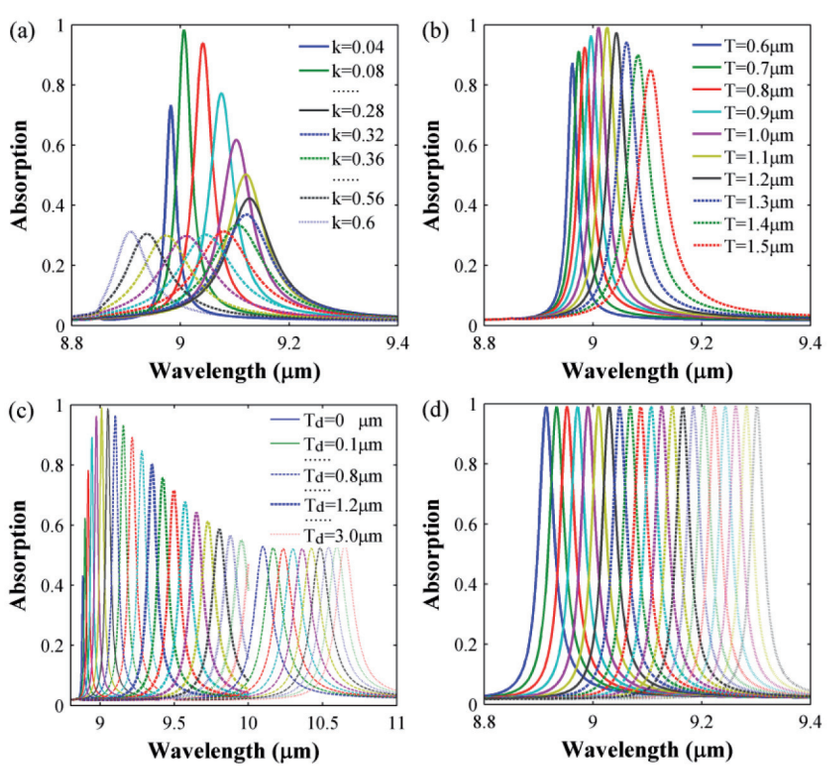

Fig. 2: Absorption Dependence on the (a) grating slit width, (b) grating thickness, (c) film thickness, and (d) grating period under normal TM-polarized incident light

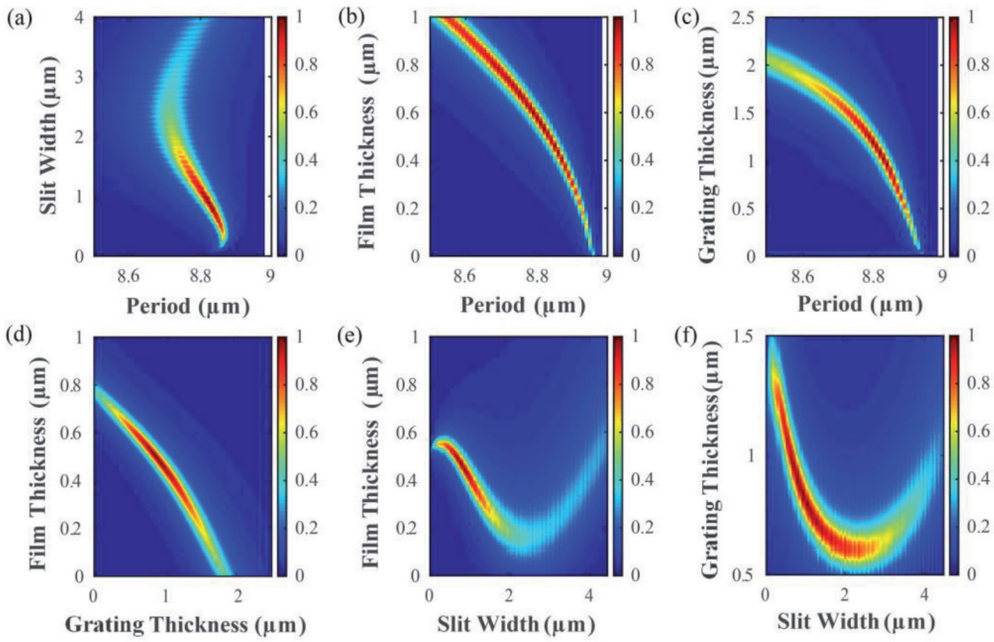

Fig. 3: Optimized geometric contour for the POA of normal TM-polarized incident light with the wavelength of 9 μm

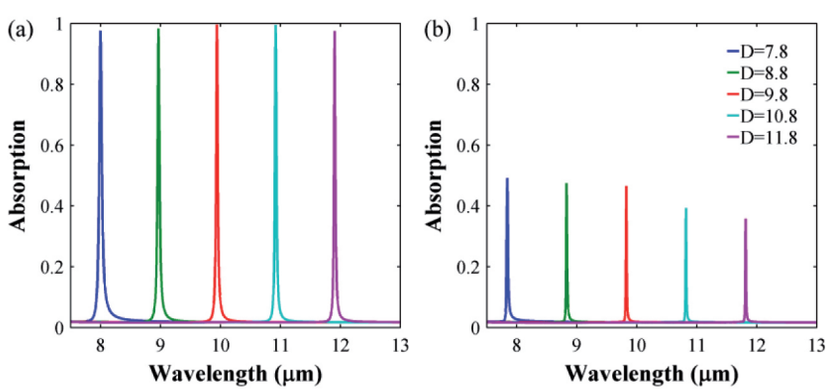

Fig. 4: Absorption spectra (a) with and (b) without the supporting film under normal TM-polarized incident light with the grating periods from 7.8 μm to 11.8 μm and the basic geometric parameters of T = 1 μm, k = 0.1 and Td = 0.5 μm

here, as its effect can be fully replaced by film thickness design. However, both the thickness and refractive index of the supporting film could be optimized for the perfect absorption.

Finally, as shown in Fig. 2(d), the linear dependence of the perfect absorption on the grating period is observed in the case of grating period D that varied from 8.75 μm to 9.15 μm by step size as 0.02 μm with other structure parameters as T = 1 μm, k = 0.086, and T_d = 0.5 μm. Considering the excitations of surface plasmon modes for thin gratings are closely related to the grating period, the relationship between the POA and surface plasmon modes excitation are obvious. The linear and broad tuning of the absorption peak presents another advantage of the structure design as the linear tunability on the POA wavelength.

For the purpose to further study the absorption dependence on the geometric parameters and get all optimized structures for a specific incident light in the far-infrared region, the influences of various geometric parameters on the perfect absorption were comprehensively considered. Fig. 3 shows the optimized geometric contour for the POA of the specific incident light with wavelength of 9 μm. The basic geometric parameters include the grating period D = 8.85 μm, grating height T = 1 μm, slit width s = 0.761 μm, and film thickness T_d = 0.5 μm.

Fig. 3(a), Fig. 3(b), and Fig. 3(c) show the perfect absorption spectra when the grating period varied from 8.5 μm to 9 μm with different slit width, film thickness and grating thickness. It is seen that the perfect absorption can be achieved when the grating period varied from 8.8 μm to 8.85 μm and slit width varied from 0.5 μm to 0.9 μm as shown in Fig. 3(a). Fig. 3(b) shows that the perfect absorption occurs when the grating period varied from 8.7 μm to 8.9 μm and film thickness varied from 0.3 μm to 0.7 μm. And Fig. 3(c) shows that the perfect absorption appear when the grating period varied from 8.8 μm to 8.85 μm and grating thickness varied from 0.7 μm to 1.1 μm. Compared the results shown in the three figures, it can be found that the range of grating period for perfect absorption is more sensitive to the influence of the grating slit width and grating thickness.

Fig. 3(d) shows the perfect absorption spectra when the grating period varied from 0 μm to 2.5 μm and the film thickness varied from 0 μm to 1 μm. As shown in Fig. 3(d) that the perfect absorption can be achieved when the grating thickness varied from 0.7 μm to 1.1 μm and film thickness varied from 0.3 μm to 0.7 μm. And the perfect absorption spectra when the grating slit width varied from 0 μm to 4.5 μm with different film thickness and grating thickness are shown in Fig. 3(e) and Fig. 3(f). Considering these three figures together, the perfect absorption can be achieved with the film thickness from 0.3 μm to 0.7 μm, grating thickness from 0.7 μm to 1.1 μm and grating slit width from 0.5 μm to 0.9 μm.

Considering all the results shown in Fig. 3, the optimized structures for the POA at λ = 9 μm are with the geometric parameters as the grating period D = 8.8-8.85 μm, film thickness T_d = 0.3-0.5 μm, grating thickness T = 0.7-1.1 μm, and slit width s = 0.5-0.9 μm. From the calculated results, the grating period is more sensitive for the POA than other parameters and the influence of the grating thickness and slit width on POA grating period range are more sensitive than the film thickness. When the grating period is determined, other parameters have approximately 50 nm tolerance. Furthermore, the optimized structure geometric parameters can be used as the fabrication windows and the film supporting grating structure can be processed by core-shell method [27], and then integrated with film together.

As the analysis for the absorption dependence on the geometric parameters, it is also demonstrated that the FP resonance in grating slits and surface plasmon excitation on the grating surfaces both contribute to the perfect absorption as it explained in the visible region case[5]. However, the film thickness case can't be explained by either FP resonant modes or surface plasmon

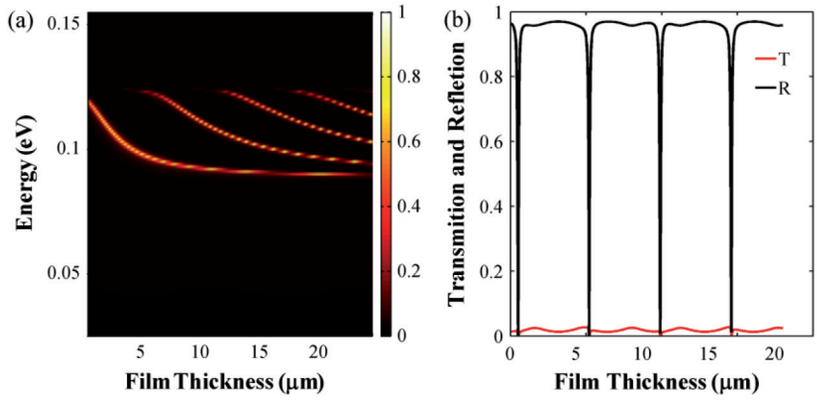

Fig. 5: (a) Absorption dependence on the incident energy and film thickness in the far-infrared region and (b) the transmittance and reflectance for a specific wavelength with different film thicknesses under the normal TM-polarized incident light at λ = 9.02 μm, and the basic geometric parameters are D = 8.85 μm, s = 0.761 μm, T = 1 μm, and Td = 0.5-18 μm

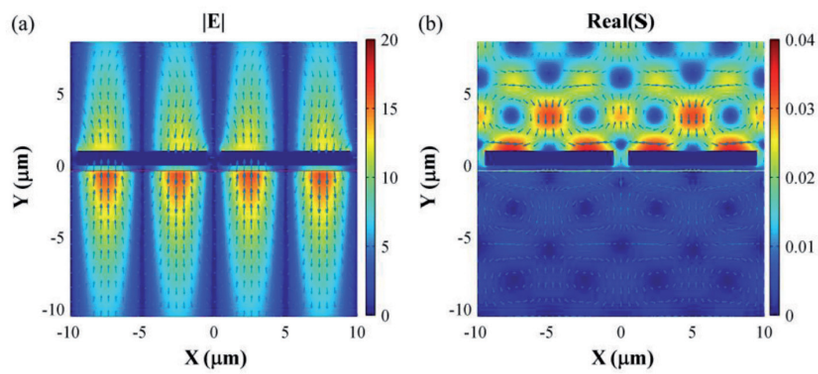

Fig. 6: (a) Electric field amplitude distribution and (b) energy flow density distribution in two periods for the POA under normal TM-polarized incident light at λ = 10.11 μm with D = 10 μm, T = 1 μm, s = 1 μm, and Td = 0.38 μm in the thin film case

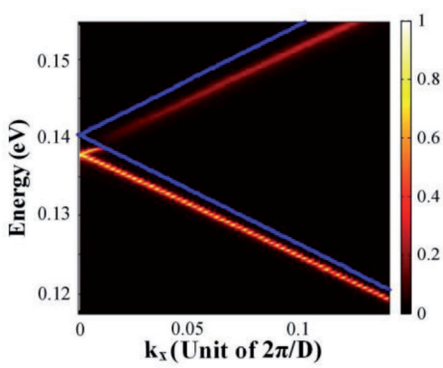

Fig. 7: Absorption dispersion in the thin film case with D = 8.85 μm, T = 1 μm, s = 1 μm, and Td = 0.38 μm, with the blue guide line denoting the dispersion of surface plasmon on the air/grating interface (also the light line in air) and the red guide line denoting the dispersion of surface plasmon on the grating/film interface (also the light line in the dielectric film)

modes. In order to understand the role of the film for the perfect absorption, the maximum absorption efficiency in the grating structure with and without film supporting were both calculated for different far-infrared wavelength and the absorption spectra are shown in Fig. 4(a) with the film thickness T_d = 0.5 μm and Fig. 4(b) without film supporting. It can be observed that near 99% absorbance can be obtained for all incident lights in the grating structures with the film supporting as shown in Fig. 4(a) and only 50% absorbance can be achieved in the grating without film supporting as shown in Fig. 4(b). It is observed from the comparison between Fig. 4(a) and Fig. 4(b) that the supporting dielectric film plays a key role in POA. A relatively narrow POA peak width indicates that the resonance lifetime must be long enough for all incident energy to dissipate in the metals.

Since the film play a key role in POA, the absorption dependence on larger film thickness range was investigated in far infrared region as shown in Fig. 5. The absorption dependence on the incident energy and film thickness is shown in Fig. 5(a). It is clearly shown that more absorption peaks appear when the film thickness increases enough, with the absorption energy located between the air/grating and grating/film surface. The POA (calculated by *A=1-T-R*) occurred periodically with the increasing film thickness, as shown in Fig. 5(b), at the film thickness T_d = 0.5, 5.2, 9.9, 14.6 μm for the specific POA incident wavelength of 9.02 μm. As shown in Fig. 5, it is seen that more POA appear when the film thickness is more than half of the incident wavelength. Thus, only redshift of the absorption peak is shown in Fig. 2(c) because the film thickness is limited in 0-3 μm, but more absorption peaks appear with more wavelength satisfied with the phase match condition when the film thickness is sufficiently large. Thus, two film thickness regions are discussed separately in the subsequent analysis as the thin film case, which the film thickness is less than half of the incident wavelength, and the thick film case, which the film thickness that is more than half of the incident wavelength.

4.2. FIELD DISTRIBUTION AND ABSORPTION DISPERSION ANALYSIS

In order to clarify the physical mechanism of the perfect absorption, especially the phase contribution in the film, the electric field distribution, energy flow density distribution, and absorption dispersion are calculated by FDTD to analyze and visualize the mechanism of POA in the far-infrared region.

(1) Thin Film Case

The electric field and energy flow density distributions in the thin film case for the POA under normal TM-polarized incident light at λ = 10.11 μm with geometric parameters of D = 10 μm, T = 1 μm, s = 1 μm, and T_d = 0.38 μm are shown in Fig. 6(a). The color and arrow length indicate the electric field amplitude, and the direction of the arrows indicate the relative ratio between amplitudes of **Ey** and **Ex**. The surface plasmon modes are strongly excited on the input and output surfaces, with asymmetric charge distributions. Although the wave guide mode in the film cannot be visualized, it is observed that the electric field on the film surface is significantly enhanced compared with that on the grating surface. In addition, the energy flow density calculated by the real part of the Poynting vector is plotted in Fig. 6(b). The arrows indicate the energy flow direction and it can be seen that the original energy flow direction is disturbed and energy vortices are formed as shown in Fig. 6(b). And the energy flow arrows end on the air/grating surface, indicating the metal absorption position.

Fig. 7 shows the absorption dispersion in the thin film case with geometric parameters of D = 8.85 μm, T = 1 μm, s = 1 μm, and

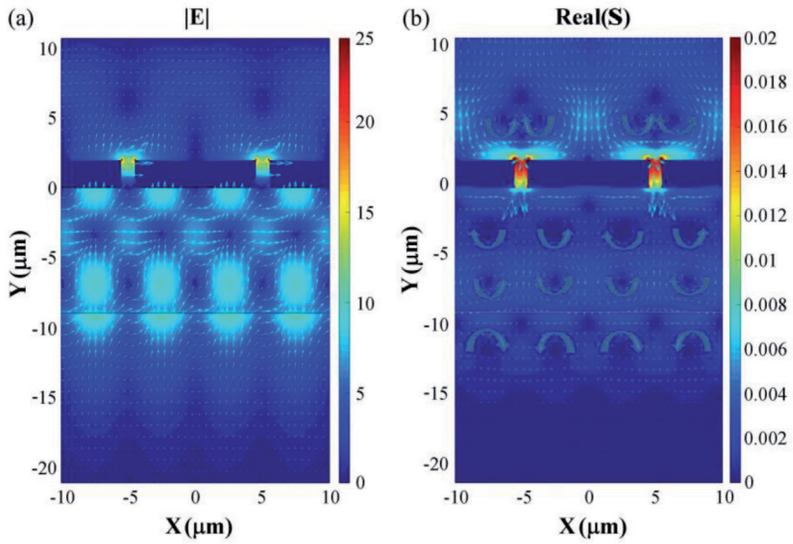

Fig. 8: (a) Electric field distribution and (b) energy flow density distribution in two periods for the POA under normal TM-polarized incident light at λ = 11.422 μm in the thick film case with D = 10 μm, T = 2 μm, s = 1 μm and Td = 9 μm

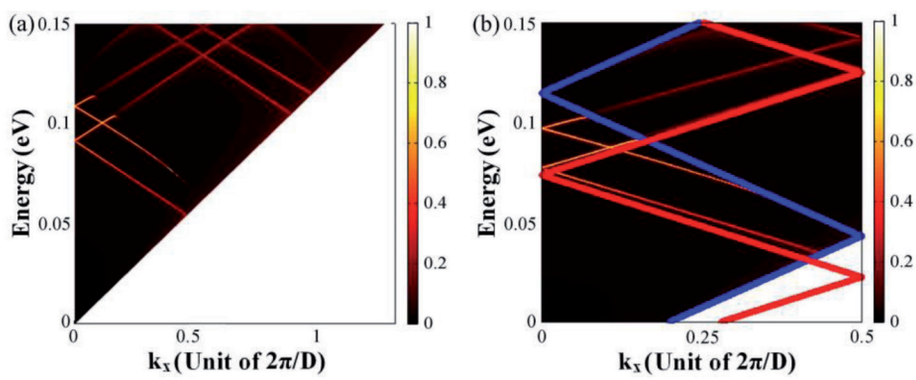

Fig. 9: (a) Absorption dispersion and (b) partial enlarged absorption dispersion and surface plasmon modes in the thick film case with D = 10 μm, T = 2 μm, s = 1 μm, and Td = 9 μm, with the blue guide line denoting the dispersion of surface plasmon on the air/grating interface (and light line in air) and red guide line denoting the dispersion of surface plasmon on the grating/film interface (and light line in the dielectric film)

T_d = 0.38 μm. The blue line is the dispersion of the surface plasmon on the air/grating interface (also the light line in air, which cannot be differentiated from the surface plasmon line), and the red line is the dispersion of the surface plasmon on the grating/film interface (also the light line in the dielectric film, which cannot be differentiated from the surface plasmon line). The deviation of the absorption dispersion is partly due to the phase contribution of the film thickness, which is further demonstrated in the thick film case.

(2) Thick Film Case

Fig. 8 shows the electric field and energy flow density distributions in the thick film case for the POA under normal TM-polarized incident light at λ = 11.422 μm with geometric parameters as D = 10 μm, T = 2 μm, T_d = 9 μm, and s = 1 μm. Compared Fig. 8(b) with the thin film case shown in Fig. 6(b), the energy flow is mainly through the slits in the thick film case rather than on the air/grating surface in the thin film case, with the corresponding electric field amplitude also shifting from the air/grating surface to the slits. This phenomenon is caused by more contributions of the grating/film surface plasmon modes and the prominent phase contribution of the film for larger thickness, thus, the POA wavelength redshifts from 10.11 μm in the thin film case to 11.422 μm in the thick film case. Fig. 8 also shows the multiple scattering waves that are bouncing back and forth in the dielectric film, which introduces a phase contribution related to film thickness.

The absorption dispersion in the thick film case with geometric parameters of D = 10 μm, T = 2 μm, s = 1 μm, and T_d = 9 μm is shown in Fig. 9. The blue and red solid lines indicate the dispersion for surface plasmon modes on the air/grating and grating/film interfaces (also the light line in air and in the dielectric film, which cannot be differentiated from the surface plasmon line), respectively. First, more absorption peaks appear as the film thickness increases in the thick film case. The multiple scattering waves in the film have no loss and only contribute the phase, thus, the narrow absorption peak feature is maintained and the absorption peak wavelength shifts from the air/grating surface plasmon mode wavelength to the grating/film surface plasmon mode wavelength with the increasing film thickness. Second, the modes on the input grating surface play a negative role in the absorption peaks, which are the so-called Rayleigh anomalies, whereas the modes on the output grating surface play a positive role in absorption. Third, the waveguide modes in the dielectric film introduce new absorption peaks, thus, the waveguide modes play a dominant role in POA. These two surface dispersion lines draw the lower and upper energy limits for resonant absorption in the thick film supporting grating structures, as clearly shown in Fig. 9.

4. CONCLUSION

A simple film supporting metallic grating structure was proposed for the demonstration of POA in the far-infrared region. The absorption dependence on geometric parameters was investigated to understand its basic properties. The features of POA in the far-infrared region were analyzed using the electric field and energy flow density distributions and absorption dispersion. The following conclusions were obtained:

(1) POA was demonstrated as near 99% absorption in the far-infrared region with the film supporting metallic grating structure as air/grating/film/air under normal TM-polarized incident light, with the advantages of linear tunability on the POA wavelength and simple structure design with a large geometric tolerance.

(2) The importance of the dielectric supporting film for POA was proven and analyzed. It was demonstrated that the dielectric supporting film introduces the asymmetric structures and provides the necessary phase contributions, which

are important for the POA phenomenon. More absorption peaks were observed when the film thickness increased.

(3) In addition to the FP resonant modes in the grating slits and the surface plasmon excitations on the grating surfaces, the waveguide modes in the dielectric film were demonstrated in the film supporting structure and even visualized in the thick film case for the perfect absorption, which significantly change the energy loss region, but with negligible effects on the POA resonant peak width. The negative role of the modes on the input grating surface and the positive role of the modes on the output grating surface were observed for the absorption.

It is significant to observe the POA in the far-infrared region, not only because of the much small skin depth for gold in the far-infrared region, but also for its potential applications in infrared sensing, detection and modulation. The advantages of the simple film supporting grating structure design for the POA in far-infrared region make it easier to implement in practical fabrication. However, the structure design is limited for TM incident light. Thus, the perfect absorption for transverse electric incident light in the far-infrared region with a simple structure design should be further investigated. In addition, the features of this phenomenon should be further investigated for the measurable conditions of the POA.

BIBLIOGRAPHY

[1] Hutley MC, Maystre D, "The total absorption of light by a diffraction grating". Optics Communications. December 1976. Vol. 19-3. p.431-436. DOI: http://dx.doi.org/10.1016/0030-4018(76)90116-4
[2] Perchec Le, Quémerais P, Barbara A, et al. "Why metallic surfaces with grooves a few nanometers deep and wide may strongly absorb visible light". Physical Review Letters. February 2008. Vol. 100-6. p.1431-1432. DOI: https://dx.doi.org/10.1103/PhysRevLett.100.066408
[3] Popov E, Maystre D, McPhedran RC, et al. "Total absorption of unpolarized light by crossed gratings". Optics Express. April 2008. Vol. 16-9. p.6146-6155. DOI: https://dx.doi.org/10.1364/OE.16.006146
[4] Kravets VG, Goldberg SN. "Plasmonic blackbody: Almost complete absorption of light in nanostructured metallic coatings". Physical Review B. November 2008. Vol. 78-20. p.2599-2604. DOI: http://dx.doi.org/10.1103/PhysRevB.78.205405
[5] Liao Y, Zhao Y. "Near-perfect absorption with a metallic grating and dielectric substrate". Journal of Nanophotonics. February 2015. Vol. 9-1. p.093087-093087-6. DOI: https://dx.doi.org/10.1117/1.JNP.9.093087
[6] Nie J, Li H, Liu W. "Perfect Anomalous Absorption of TM Polarized Light in Metallic Grating Situated in Asymmetric Surroundings". IEEE Photonics Journal. December 2014. Vol. 6-6. p.1-8. DOI: https://dx.doi.org/10.1109/JPHOT.2014.2363439
[7] Wang Y, Sun TY, Paudel T. "Metamaterial-plasmonic absorber structure for high efficiency amorphous silicon solar cells". Nano Letters. December 2011. Vol. 12-1. p.440-445. DOI: https://dx.doi.org/10.1021/nl203763k
[8] Abass A, Le KQ, Alù A, et al. "Dual-interface gratings for broadband absorption enhancement in thin-film solar cells". Physical Review B Condensed Matter. March 2012. Vol. 85-11. p.115449-115449-8. DOI: https://dx.doi.org/10.1103/PhysRevB.85.115449
[9] Ameling R, Langguth L, Hentschel M, et al. "Cavity-enhanced localized plasmon resonance sensing". Applied Physics Letters. December 2010. Vol. 97-25. p. 2531161-2531161-3. DOI: https://dx.doi.org/10.1063/1.3530795
[10] Rosenberg J, Shenoi RV, Vandervelde TE. "A multispectral and polarization-selective surface-plasmon resonant midinfrared detector". Applied Physics Letters. October 2009. Vol. 95-16. p.161101-161101-3. DOI: https://dx.doi.org/10.1063/1.3244204
[11] Diem M, Koschny T, Soukoulis CM. "Wide-angle perfect absorber/thermal emitter in the terahertz regime". Physical Review B. July 2008. Vol. 79-3. p.033101-033101-4. DOI: https://dx.doi.org/10.1103/PhysRevB.79.033101
[12] Brongersma ML, Halas NJ, Nordlander P. "Plasmon-induced hot carrier science and technology". Nature Nanotechnology. January 2015. Vol.10-1 p.25-34. DOI: https://dx.doi.org/10.1038/nnano.2014.311
[13] Tan WC, Sambles JR, Preist TW. "Double-period zero-order metal gratings as effective selective absorbers". Physical Review B. May 2000. Vol. 61-19. p. 13177-13182. DOI: https://dx.doi.org/10.1103/PhysRevB.61.13177
[14] Pendry JB, Martín-Moreno L, Garcia-Vidal FJ. "Mimicking surface plasmons with structured surfaces". Science. September 2004. Vol. 305-5685. p.847-848. DOI: https://dx.doi.org/10.1126/science.1098999
[15] Huang XR, Peng RW, Fan RH. "Making metals transparent for white light by spoof surface plasmons". Physical Review Letters. December 2010. Vol. 105-24. p.119-127. DOI: https://dx.doi.org/10.1103/PhysRevLett.105.243901
[16] Garcia-Vidal FJ, Martin-Moreno L, Ebbesen TW, et al. "Light passing through subwavelength apertures". Reviews of Modern Physics. March 2010. Vol. 82-1. p.729-787. DOI: https://dx.doi.org/10.1103/RevModPhys.82.729
[17] Liu X, Starr T, Starr AF, et al. "Infrared spatial and frequency selective metamaterial with near-unity absorbance". Physical Review Letters. May 2010. Vol. 104-20. p.207403-207403-4. DOI: https://dx.doi.org/10.1103/PhysRevLett.104.207403
[18] Aydin K, Ferry VE, Briggs RM, et al. "Broadband polarization-independent resonant light absorption using ultrathin plasmonic super absorbers". Nature Communications. November 2011. Vol. 2-1. p. 193-198. DOI: https://dx.doi.org/10.1038/ncomms1528
[19] Rogalski A. "Thermopiles". Infrared Detectors, 2nd ed.,. FL. CRC Press 2011.
[20] Liu N, Mesch M, Weiss T, et al. "Infrared perfect absorber and its application as plasmonic sensor". Nano Letters. July 2010. Vol. 10-7. p. 2342-2348. DOI: https://dx.doi.org/10.1021/nl9041033
[21] Chen Y, Li X, Luo X, et al. "Tunable near-infrared plasmonic perfect absorber based on phase-change materials". Photonics Research. June 2015. Vol. 3-3. p.54-57. DOI: https://dx.doi.org/10.1364/PRJ.3.000054
[22] Kang GG, Vartiainen I, Bai BF, et al. "Enhanced dual-band infrared absorption in a Fabry-Perot cavity with subwavelength metallic grating". Optics Express. January 2011. Vol. 19-2. p.770-778. DOI: https://dx.doi.org/10.1364/OE.19.000770
[23] Gao H, Gu C, Zheng ZY, et al. "Nearly perfect absorption in a single-layer metallic grating with rectangular grooves on its front surface". Applied Physics B. December 2014. Vol. 117-3. p.875-883. DOI: https://dx.doi.org/10.1007/s00340-014-5903-1
[24] Collin S, Pardo F, Teissier R, et al. "Horizontal and vertical surface resonances in transmission metallic gratings". Journal of Optics A pure & Applied Optics. August 2002. Vol. 4-5. p.S154-S160. DOI: https://dx.doi.org/10.1088/1464-4258/4/5/364
[25] Innovation KJ. "GD-Calc". February 2016. http://www.kjinnovation.com/
[26] Jackson JD. "Maxwell Equations, Macroscopic Electromagnetism, Conservastion Laws". Classical Electrodynamics, 3rd ed., Wiley. 1999
[27] Collin S, Vincent G, Haidar R, et al. "Nearly perfect fano transmission resonances through nanoslits drilled in a metallic membrane". Physical Review Letters. January 2010. Vol. 104-2. p.358-359. DOI: https://dx.doi.org/10.1103/PhysRevLett.104.027401.

APPRECIATION

This work was supported by the Ministry of Science and Technology of China (Grant No. 2015CB932400), and the National Natural Science Foundation of China (Grant Nos. 11404247, 11134013, 11227407).